

A van der Waals Heterostructure with an Electronically Textured Moiré Pattern: PtSe₂/PtTe₂

Jingfeng Li, Mahdi Ghorbani-Asl, Kinga Lasek, Vimukthi Pathirage, Arkady V. Krasheninnikov, and Matthias Batzill*



Cite This: *ACS Nano* 2023, 17, 5913–5920



Read Online

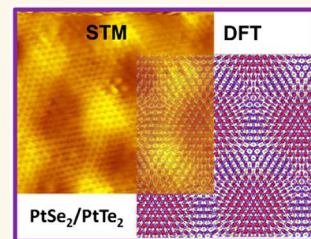
ACCESS |

Metrics & More

Article Recommendations

Supporting Information

ABSTRACT: The interlayer interaction in Pt-dichalcogenides strongly affects their electronic structures. The modulations of the interlayer atom-coordination in vertical heterostructures based on these materials are expected to laterally modify these interlayer interactions and thus provide an opportunity to texture the electronic structure. To determine the effects of local variation of the interlayer atom coordination on the electronic structure of PtSe₂, van der Waals heterostructures of PtSe₂ and PtTe₂ have been synthesized by molecular beam epitaxy. The heterostructure forms a coincidence lattice with 13 unit cells of PtSe₂ matching 12 unit cells of PtTe₂, forming a moiré superstructure. The interaction with PtTe₂ reduces the band gap of PtSe₂ monolayers from 1.8 eV to 0.5 eV. While the band gap is uniform across the moiré unit cell, scanning tunneling spectroscopy and dI/dV mapping identify gap states that are localized within certain regions of the moiré unit cell. Deep states associated with chalcogen *p*_z-orbitals at binding energies of \sim 2 eV also exhibit lateral variation within the moiré unit cell, indicative of varying interlayer chalcogen interactions. Density functional theory calculations indicate that local variations in atom coordination in the moiré unit cell cause variations in the charge transfer from PtTe₂ to PtSe₂, thus affecting the value of the interface dipole. Experimentally this is confirmed by measuring the local work function by field emission resonance spectroscopy, which reveals a large work function modulation of \sim 0.5 eV within the moiré structure. These results show that the local coordination variation of the chalcogen atoms in the PtSe₂/PtTe₂ van der Waals heterostructure induces a nanoscale electronic structure texture in PtSe₂.



KEYWORDS: *van der Waals heterostructure, moiré pattern, scanning tunneling microscopy, work function, PtSe₂, transition metal dichalcogenide*

One of the most exciting features of van der Waals (vdW) heterostructures is the formation of moiré structures due to long-range coincidence lattices formed by the combination of materials with different lattice constants or rotation (twist) angles. Despite weak interlayer interactions, different relative atom positions within the moiré unit cell cause a periodic potential that modifies the electronic structure of the two-dimensional (2D) materials. These moiré patterns in vdW heterostructures thus allow an additional degree of engineering of materials properties, which has been utilized to demonstrate unconventional materials design principles and their potential applications. Some properties have emerged due to moiré super-periodicities in vdW heterostructures: (i) the lateral moiré superstructure gives rise to superlattice Dirac points and consequently Hofstadter butterfly states. This has been observed in hexagonal boron nitride (h-BN)/graphene vdW heterostructures.^{1,2} (ii) Moiré structures formed by twisting two graphene lattices result in strongly correlated Mott insulator or superconducting states at precisely controlled twist angles.^{3–5} (iii) In semiconducting

transition metal dichalcogenide (TMD) heterostructures, interlayer interactions induce local modulations of their band gaps^{6,7} that may cause flat bands,^{8,9} quantized confined states,¹⁰ and optical excitations of the so-called moiré excitons.^{11,12} Here we explore another periodic texturing in the electronic properties induced by moiré superlattice in vdW heterostructures in the form of lateral work function modulations. To accomplish strong work function modulations in the moiré structures, the interlayer charge redistribution must depend on local interlayer atom coordination within the moiré unit cell. This has been shown for monolayer materials deposited on crystalline supports such as NaCl,¹³ FeO,^{14,15} or

Received: December 29, 2022

Accepted: March 14, 2023

Published: March 17, 2023



ACS Publications

© 2023 American Chemical Society

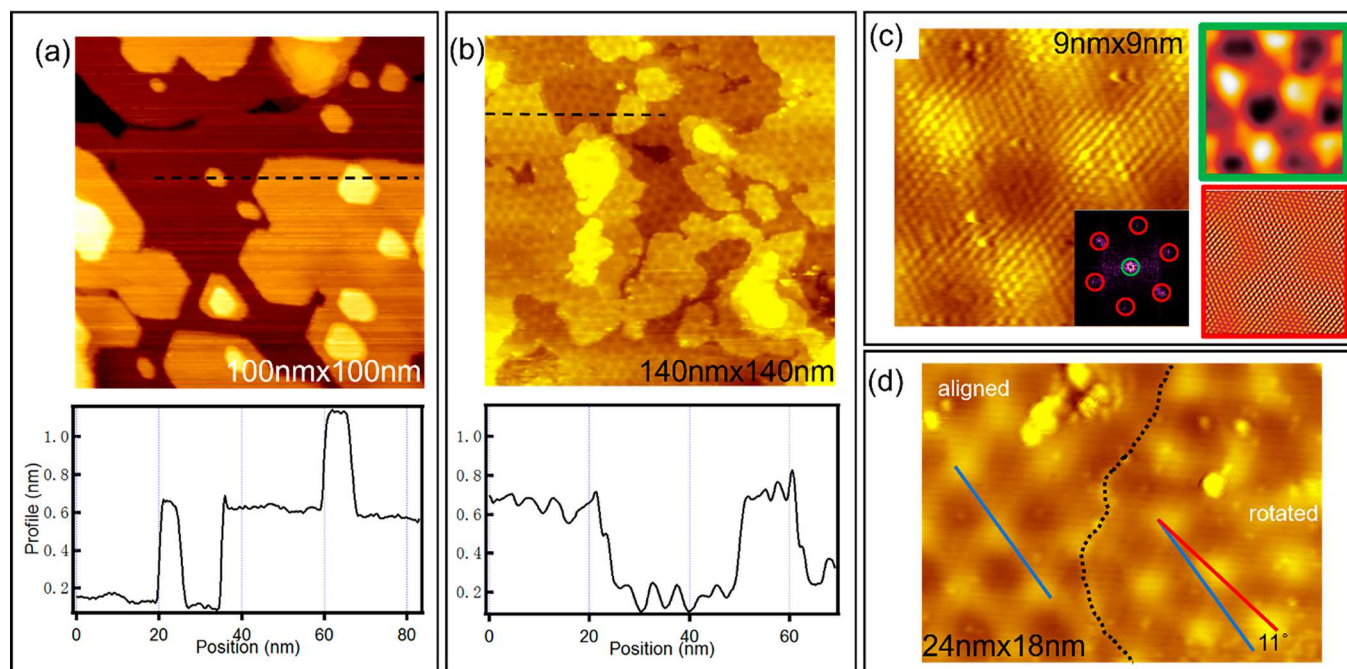


Figure 1. STM characterization of the morphology of a PtSe₂/PtTe₂ heterostructure. (a) PtTe₂ multilayers on HOPG, which serves as the substrate for PtSe₂ growth. The line profile along the dashed line is shown in the bottom panel and shows step heights corresponding to the interlayer separation of PtTe₂. (b) STM image of monolayer PtSe₂ on PtTe₂. The surface is uniformly covered with a moiré structure, and the step heights correspond to those of the underlying PtTe₂ substrate. The black dashed lines indicate the location of the line profiles shown in the bottom panel. Tunneling condition $V_{\text{bias}} = 3$ V, $I_t = 0.2$ nA. (c) High-resolution STM image of the moiré structure and its Fourier transformations (a larger version of the Fourier transformation can be found in Figure S3). The red and green circles in the Fourier transformation indicate the atomic and moiré periodicity, respectively, and the corresponding Fourier-filtered images are shown. Tunneling condition $V_{\text{bias}} = 0.5$ V, $I_t = 0.1$ nA. (d) Two observed moiré structures, separated by the dashed line. These two moiré structures originate from a small rotation of the PtSe₂ lattice with respect to the PtTe₂ substrate. The red and blue lines indicate the direction of the moiré unit cell, which illustrates the roughly 11° rotation between these two moiré unit cell directions. Tunneling condition $V_{\text{bias}} = 3$ V, $I_t = 0.2$ nA.

Pb¹⁶ monolayers on silver, platinum, or silicon crystals, respectively. More prominently this effect has been also explored for graphene on Rh¹⁷ or h-BN on various transition metals (e.g., Rh,¹⁸ Ru,¹⁹ Cu,^{20,21} Ir²²) where the varying coordination of the BN atoms with respect to the surface metals gives rise to strongly variable chemical interactions, causing large corrugation of the h-BN layer and consequently modulations of interlayer dipoles and the local work function.²³ Subsequently, it was also shown that the work function modulation of such a h-BN monolayer on a metal substrate can be transferred further to a semiconducting MoSe₂ layer epitaxially grown on the h-BN/metal substrate.²⁴ In this study we are aiming to establish such electronic modulations in a pure, potentially free-standing vdW system, i.e., averting a 3D metal substrate. In order to achieve the strongly modulated interlayer interactions that can cause the desired work function modulations, we explore the platinum dichalcogenide system, which has demonstrated extraordinary layer-dependencies of the electronic structure.^{25–29} PtSe₂ and PtTe₂ exhibit band gaps of 1.8 eV and 0.5 eV, respectively, as monolayers³⁰ but become semi-metals for multilayer samples, indicating the strong dependence of their electronic structure on interlayer interactions. This dependence on interlayer interaction makes them promising materials for studying the effects of moiré structures on the electronic properties in vdW heterostructures. Moreover, the work function variation within a moiré unit cell is more pronounced for larger unit cells,¹⁵ which can be achieved by appropriate differences in the lattice constants. The larger lattice constants of tellurides versus selenides of the

same transition metal make their combination into heterostructures ideal for creating such moiré patterns. Here we show that the electronic structure of a PtSe₂ monolayer grown on PtTe₂ is modulated by the varying interlayer interaction in the moiré pattern, and the work function in the PtSe₂/PtTe₂ heterostructure is indeed strongly modulated by close to 0.5 eV within the moiré unit cell. Thus, this demonstrates an electronically textured moiré pattern in a pure vdW heterostructure system.

RESULTS AND DISCUSSION

PtSe₂ monolayers are synthesized on PtTe₂ ultrathin films by molecular beam epitaxy (MBE). Figure 1(a) shows a large-scale scanning tunneling microscopy (STM) image of a few-layer PtTe₂ film grown on a highly oriented pyrolytic graphite (HOPG) substrate. PtTe₂ films on HOPG exhibits large flat terraces with terrace steps of only ~0.4 nm height, corresponding to the interlayer separation between PtTe₂ van der Waals layers. This film is used as a substrate for PtSe₂ growth. Interestingly, PtSe₂ grows in a Stranski–Krastanov-like growth mode, with the first monolayer wetting the surface and subsequent growth resulting in cluster formation; see Supporting Information, Figure S1. While such a growth for 2D materials is unusual and its mechanism is not well understood for this system, it facilitates the study of monolayer PtSe₂ on PtTe₂ films. Figure 1(b) shows the deposition of close to one monolayer of PtSe₂ on the PtTe₂ substrate. The surface exhibits the same atomic height steps as for pure PtTe₂, suggesting that the step-structure of the

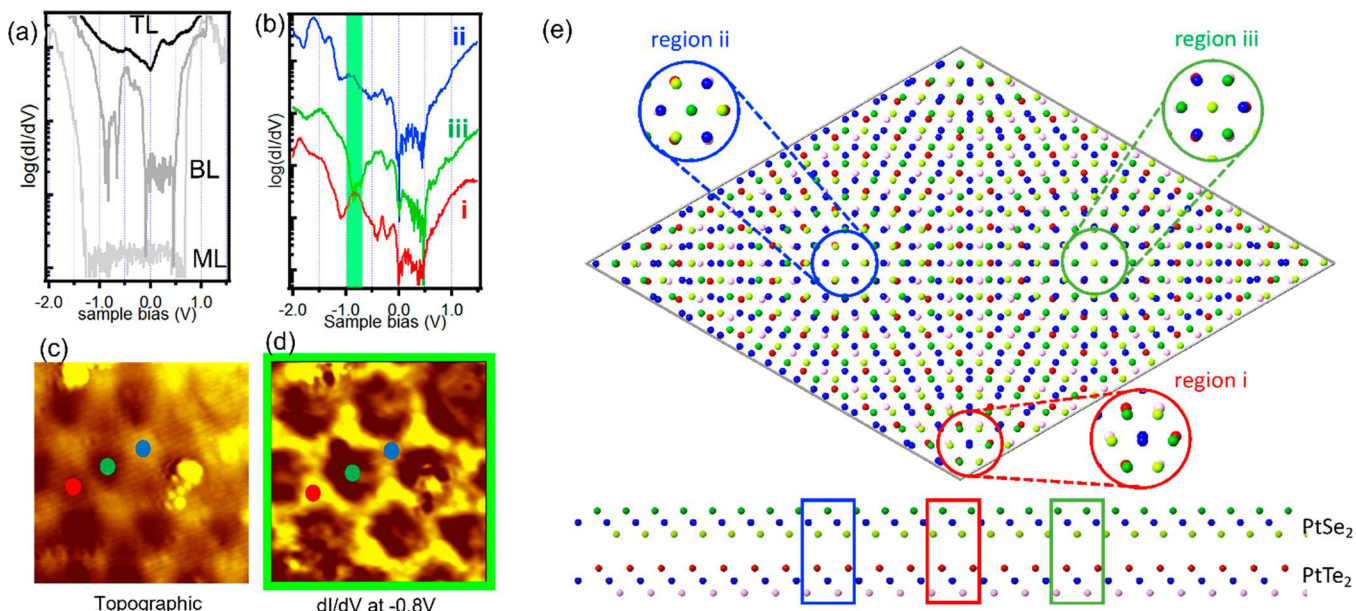


Figure 2. Electronic structure of PtSe_2 . (a) Layer dependence of the dI/dV spectra of PtSe_2 grown on a HOPG substrate. STM images of PtSe_2 islands and location of the STS spectra are shown in Figure S4. The monolayer (ML) exhibits a large band gap of 1.8 eV, the bilayer (BL) has a band gap of 0.6 eV, and the trilayer (TL) is metallic. (b) Selected dI/dV spectra of PtSe_2 monolayer on PtTe_2 substrate at high-symmetry sites of the moiré structure (set point for STS: $I = 100 \text{ pA}$, $V = 0.6 \text{ V}$). The dI/dV spectra are plotted on a log-scale; the same spectra in (a) and (b) can be found plotted on a linear scale in Figure S6. The position at which the color-coded spectra were taken is also indicated in the STM image shown in (c). A dI/dV map taken at -0.8 eV of the same region is shown in (d), highlighting the localized distribution of the electronic state at -0.8 eV . The atomic structure model of the moiré unit cell is presented in (e); a detailed description of the three symmetry sites can be found in the text.

underlying PtTe_2 substrate is not affected by the PtSe_2 growth. The surface now exhibits a moiré pattern whose periodic modulation is observed in the STM images. Figure 1(c) shows a high-resolution STM image of the moiré structure and its Fourier transformation with the corresponding Fourier-filtered images. From Figure 1(c) the moiré unit cell is determined to consist of 13 PtSe_2 unit cells, which is consistent with a close coincidence lattice of $13 \times a_{\text{PtSe}_2}$ ($13 \times 0.38 \text{ nm} = 4.94 \text{ nm}$) on $12 \times a_{\text{PtTe}_2}$ ($12 \times 0.41 \text{ nm} = 4.92 \text{ nm}$). In addition to this majority moiré structure formed by the van der Waals heterostructure of rotationally aligned PtSe_2 and PtTe_2 lattices, a slightly rotated structure is also observed. These two moiré structures are rotated by $\sim 11^\circ$ relative to each other, as shown in Figure 1(d). The rotation angles of the moiré unit cells amplify small rotations of the atomic lattices, and an 11° rotation of the moiré unit cells corresponds to only a $\sim 1^\circ$ rotation of the atomic lattices (see Figure S2) so that the grown PtSe_2 monolayer is still roughly aligned with the PtTe_2 substrate. The amplification of the rotation of the moiré structure also enables us to identify the aligned from the rotated PtSe_2 monolayer. If the PtSe_2 monolayer is aligned with the PtTe_2 substrate, the atomic unit cell of PtSe_2 is also aligned with the moiré unit cell, while if the PtSe_2 layer is rotated by $\sim 1^\circ$ relative to the PtTe_2 substrate, then the moiré unit cell is rotated by $\sim 10^\circ$ relative to the PtSe_2 unit cell, which can be observed in atomic resolution images. Generally, the order and long-range coherence of the moiré structure in this $\text{PtSe}_2/\text{PtTe}_2$ system are less than in many of the related moiré patterns of monolayer films on metal supports discussed above. One possible reason is the lower synthesis temperature for this system, which is limited to $\sim 300^\circ \text{C}$. At higher growth temperatures an intermixing of the PtSe_2 with the PtTe_2

substrate is observed. The relatively low thermal stability of these phases has also been reported for pure PtTe_2 , which results in easy loss of Te and transformation into different compositional phases upon vacuum annealing.³¹

Interface States. PtSe_2 exhibits strong layer-dependent electronic properties. Scanning tunneling spectroscopy (STS) measurements for mono-, bi-, and trilayer PtSe_2 exhibit band gaps of 1.8 eV, 0.6 eV, and 0 eV, respectively, as shown in Figure 2(a) for PtSe_2 layers grown directly on the HOPG substrate. These extraordinarily strong variations are due to interlayer interactions in the Pt-dichalcogenide family. This raises the question of how the interlayer interactions affect the electronic structure of a monolayer PtSe_2 . The interlayer interactions are dominated by the frontier p -orbitals of the chalcogen atoms, whose overlap in the vdW gap gives rise to the closing of the band gaps in the pure materials. In the heterostructure, interlayer interactions may be dominated by the $4p$ - and $3p$ -orbitals of Te and Se atoms, respectively. Thus, the interaction between the different chalcogen atoms and their spatially varying coordination within the moiré structure is anticipated to contribute to local electronic structure variation within the moiré unit cell. STS measurements of the electronic structure of monolayer PtSe_2 on PtTe_2 in different regions of the moiré unit cell are shown in Figure 2(b). We consider three high-symmetry sites of the moiré structure as follows: (i) sites where PtSe_2 is in registry with PtTe_2 , i.e., the two structures form a 1T-stacking, and therefore denoted “1T site”; (ii) sites where Se atoms are on top of Te atoms, denoted as “Se-Te site”, and (iii) sites where Se atoms are over the Pt sites in the PtTe_2 layer, thus denoted “Se-Pt site”. These three sites are illustrated in Figure 2(e). It can be seen that, similar to bilayer PtSe_2 , the band gap in monolayer PtSe_2 on PtTe_2 is also narrowed as compared to

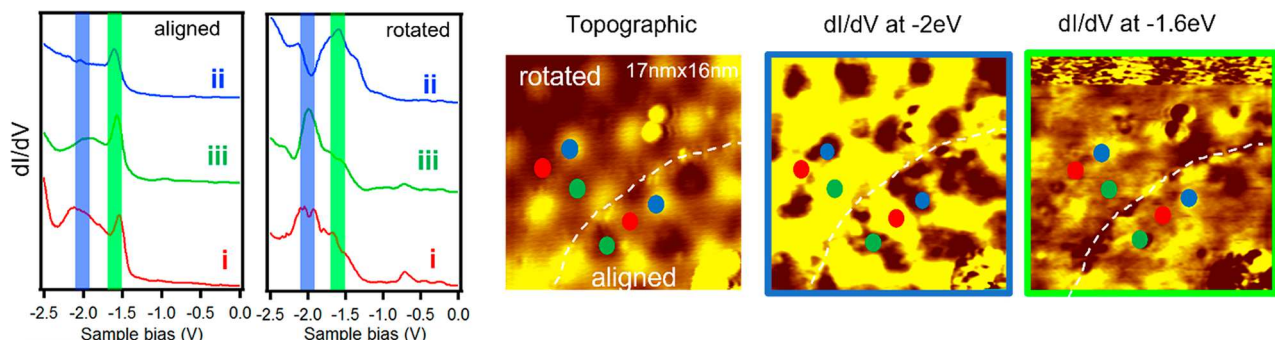


Figure 3. dI/dV spectroscopy of deep states for different positions in the two moiré structures (set point for STS: $I = 100$ pA, 1 V). For modulations of shallow states in the rotated domains, detailed spectra are shown in Figure S5. Two main states can be identified at -1.6 eV and -2 eV, which may be attributed to p_{xy} - and p_z -derived selenium states, respectively. The STM image (tunneling condition: $V_{bias} = 3$ V, $I_t = 0.2$ nA) shows both aligned and rotated moiré domains. The domain boundary is indicated by the dashed line. The state at -2 eV exhibits a stronger localization within regions I and III, while it is absent in region II. The state at -1.6 eV is less modulated within the moiré structure, supporting the assignment to p_{xy} -derived states.

quasi-freestanding PtSe_2 monolayers grown on a HOPG substrate, but a band gap, similar to that observed for bilayer PtSe_2 , of ~ 0.5 eV remains. This indicates that the interlayer interactions between PtSe_2 and PtTe_2 have similar effects on the gap as in PtSe_2 – PtSe_2 contacts. While the band gap narrowing of monolayer PtSe_2 on PtTe_2 , compared to freestanding monolayer PtSe_2 , is uniform across the moiré unit cell, there are variations in the local density of states (LDOS) within different regions of the moiré unit cell. Electronic states can be identified with a strong variation at -0.8 eV below the Fermi level, as reflected in the dI/dV map. These states at -0.8 eV binding energy are most pronounced at region I and absent at region III. We demonstrate its localization by comparing the topographic STM image with dI/dV mapping shown in Figure 2(c) and (d), respectively. Comparison of the aligned with that of the slightly rotated PtSe_2 moiré structure shows that the states at -0.8 eV show an even stronger localization at region II in the moiré unit cell (see Figure S5).

Electronic states within an energy window for which the free-standing PtSe_2 monolayer exhibits a band gap can be attributed as originating from the interlayer interaction with the PtTe_2 substrate. In addition to these “shallow” states, we also observe lateral modulations of electronic states farther away from the Fermi level. These deep states are shown in Figure 3 for a region that shows moiré structures due to both a PtSe_2 domain that is aligned with PtTe_2 and a domain with a slight rotation of the PtSe_2 layer with respect to PtTe_2 . Electronic states at -1.6 eV and -2 eV are clearly discerned in the dI/dV spectroscopy. Based on previous calculations, these states are associated with p_{xy} and p_z chalcogen orbitals, respectively.³² Modulations of these states are observed for both moiré structures but are more pronounced in the domains where the PtSe_2 is rotated with respect to the PtTe_2 . The p_z state at -2 eV is observed in regions I and III of the aligned moiré but is suppressed in region II. This suggests that the states associated with p_z orbitals are altered if the chalcogen atoms in the two layers are on top of each other. In contrast, the states at -1.6 eV are associated with p_{xy} orbitals, and those are less affected in the moiré structure. Interestingly, the p_z states have been associated with a spin texture of PtSe_2 monolayers,²⁷ and thus their modulation in the moiré structure implies a local modulation also of this spin texture.

Work Function. Determining work function variations in nanoscale structures by field emission resonance (FER)

spectroscopy has been widely used in STM.^{13–24,33–35} Briefly, in FER the bias voltage between the STM tip and the sample surface is chosen such that the Fermi level of the STM tip lies above the vacuum level of the sample. In this Fowler–Nordheim tunneling regime, the drop in the potential at the tunnel junction causes a potential well between the tip and the sample surface. The quantum-confined image potential states in this quantum well are probed in FER spectroscopy. Local changes in the substrate work function modify the image potential states, and thus a shift of the resonance states is a direct measure of the work function modulations along the surface. It is generally challenging to determine absolute values of the work function because the STM tip properties are not well-defined, but for a stable tip the relative changes for different substrate sites are given by the shift of the resonance states.

Figure 4 shows FERs at different positions along a line across the moiré unit cell. All FERs, apart from the lowest energy one, which is known to be unreliable,^{20,23,24} shift by approximately the same amount. Reported evidence suggests that the second FER is the most relevant for measuring work function variations,³⁶ and therefore the reported values refer to the second FER. The largest work function is observed for region II, which is 0.48 eV larger than that for region III. Region I is in between, with a work function 0.28 eV lower than that of region II. Slightly less work function modulations are observed for the rotated moiré structure, as shown in Figure S7. This is a substantial work function difference and the first reported for a TMD vdW heterostructure. Strong modulations of the work function imply surface dipoles that must originate from interlayer charge transfer in the PtSe_2 – PtTe_2 heterostructure. To gain further insight into the experimentally observed work function modulations, density functional theory (DFT) calculations of the local electronic structure and charge transfer within the moiré structure have been performed, which is discussed next.

PtSe₂/PtTe₂ Moiré Structure and Electronic Properties from DFT Calculations. To obtain deeper insights into the atomic structure of the interface, we performed extensive DFT calculations using an unsupported PtSe_2 – PtTe_2 supercell as a model heterostructure; see the **Methods** for details. A supercell with a single PtTe_2 layer, rather than multilayers as in the experiments, is necessitated by the computational limitations imposed by the large number of heavy atoms in

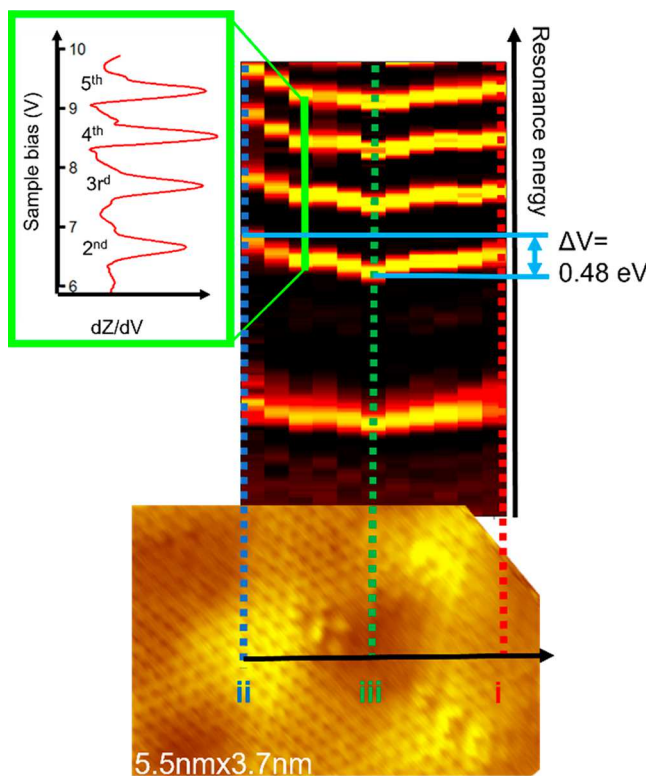


Figure 4. Work function modulation within a moiré unit cell measured by field emission resonance (FER) spectroscopy. FER spectra are measured along the moiré unit cell from regions ii to iii to i. One spectrum is shown as an example, and the others are plotted as an intensity map to illustrate the variation of the resonances as a function of the position. The largest resonance energy difference is observed between regions ii and iii and is measured to be 0.48 eV. The strong variations of the FER at different sites of the moiré unit cell demonstrate the work function modulation within the moiré unit cell. The imaging conditions for the STM data are $V_{\text{bias}} = 0.5$ V, $I_t = 0.1$ nA.

the structure. Test simulations on a smaller unit cell with rotated PtSe₂/PtTe₂ layers show that the band gap of monolayer PtSe₂ is not changed by the number of supporting PtTe₂ layers (Figure S8). This illustrates that the monolayer PtTe₂ can be a reasonable model system to qualitatively describe the behavior in the experimental system. The computed relaxed crystal structure exhibits only very weak topographical buckling of the bilayer structure, implying that the observed apparent topography in STM images is likely associated with an electronic contrast; however, this needs to be verified by structural probes.

Depending on the relative positions of the interface Se atoms in the PtSe₂ with respect to the interface Te atoms in the PtTe₂ monolayer, see Figure 2(e), the Se–Te interatomic distances and angles are different in different regions of the moiré pattern. As a result, the local interactions between the layers is different, giving rise to the variation of the local electronic structure. Figure 5(a) shows the LDOS at three moiré sites in the heterostructure. The calculated band gap edge energies of the PtSe₂/PtTe₂ heterostructure are almost unchanged for the different sites within the moiré structure, with only small variations of less than 30 meV (see Figure S9), and thus the “local” band gap remains nearly constant within the moiré unit cell (note that the calculated band gap energy depends sensitively on inclusion of spin–orbit coupling in the

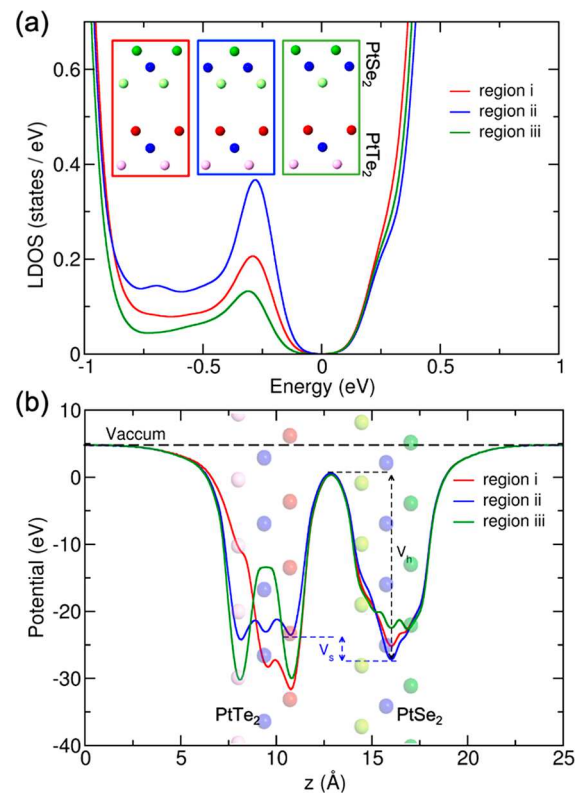


Figure 5. (a) Local density of states for different regions in the moiré structures of the PtSe₂/PtTe₂ heterostructure. The LDOS is shown for PtSe₂. (b) Electrostatic potential along the direction perpendicular to the heterostructure and averaged within planes parallel to the heterostructure.

calculations, see Table S1). The LDOS below the Fermi level (at about -0.3 eV) is larger in region ii as compared to the other sites. The constant band gap is consistent with the experimental STS data. Also, the variation of the LDOS at the band edge is consistent with the STM apparent topographic appearance (see Figure 2(c)) of the heterostructure, indicating higher tunneling contrast in region ii than in the other two moiré regions. We further analyzed the modulation of the averaged electrostatic profile perpendicular to the heterostructure at different sites in the moiré structure, Figure 5(b), where the differences are evident. The variation of the electrostatic potential at different sites is caused by the amount of charge transfer at the specific interface area. Our results indicate that the potential height V_h at the PtSe₂ layer is larger in region ii than in the other two regions. This is consistent with the calculated Bader charges transferred from PtTe₂ to PtSe₂, which were found to be 4×10^{-3} , 7×10^{-3} , and 2×10^{-3} electrons/atoms for regions i, ii, and iii, respectively (see Figure 6). The charge transfer from PtTe₂ to PtSe₂ is related to the difference in the work functions, which can be described by the relation $Q \propto \Delta\varphi$, where Q represents the charge and $\Delta\varphi$ is the difference in the work functions between the two monolayers.³⁷ These charge transfers can be associated with the experimentally measured work function modulations. Since the native PtSe₂ bilayer does not exhibit such work function modulations, such behavior in the heterostructure can be attributed solely to charge-transfer-induced dipoles at the PtSe₂/PtTe₂ interface.

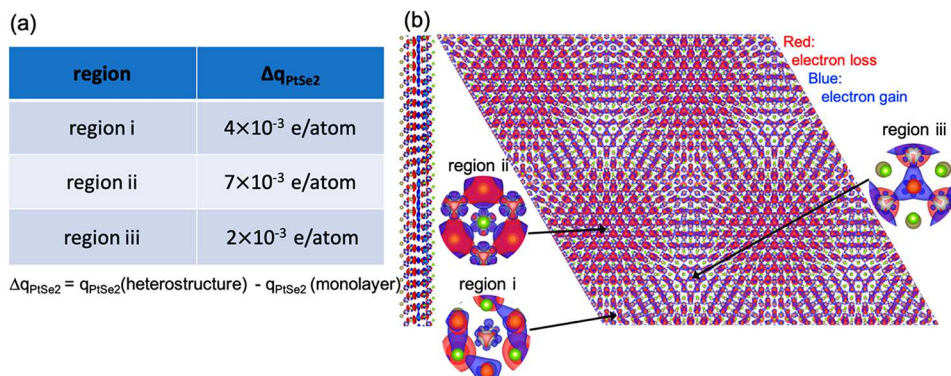


Figure 6. (a) Average Bader charges at each region in the $\text{PtSe}_2/\text{PtTe}_2$ heterostructure with PtSe_2 being on top, as compared to the isolated PtSe_2 monolayer. (b) Charge transfer between PtSe_2 and PtTe_2 layers calculated as the difference between the charges in the heterostructure and the isolated monolayers. Blue and red represent charge accumulation and charge depletion. Note the variation of charge in different areas of the moiré pattern.

CONCLUSION

In conclusion, we have shown that the $\text{PtSe}_2/\text{PtTe}_2$ vdW heterostructure is a strongly electronically corrugated moiré system, as evident from the experimental STM/STS data. Even with relatively weak interlayer interactions in a pure vdW bilayer, the varying interlayer atom configurations within the moiré unit cell have pronounced effects on the local electronic structure. STS shows that the atom coordination between the two materials causes interlayer states that vary within the moiré structure, and their localization is imaged by dI/dV mapping. The varying interactions of the chalcogen p -orbitals in the $\text{PtSe}_2/\text{PtTe}_2$ moiré unit cell give rise to varying interface dipoles and thus different local work functions. This has been experimentally determined by FER spectroscopy, and work function shifts close to 0.5 eV have been observed for the different local stacking configurations. The strong local modulation of the work function implies that in-plane dipoles permit the electrostatic potential offsets. Surface dipoles and work function variations have been shown to facilitate the alignment of molecular adsorbates on h-BN/metal substrates^{38–42} and the control over the adsorbate charge transfer within the moiré structure,^{43,44} and similar effects can be anticipated for this purely vdW heterostructure. Pt-dichalcogenides have also shown promise for hydrogen evolution and oxygen reduction electrocatalysis.^{45–47} Work function engineering by the formation of vdW heterostructures is an approach to tune their surface chemical properties, and thus vdW heterostructures may be anticipated to exhibit varying and intriguing electrocatalytic properties as compared to their individual components. Moreover, the Pt-chalcogenides are known for their spin textures^{27,48} and magnetic properties,^{49,50} and the interaction of the local spins with the periodic moiré dipoles may give rise to magnetic properties modulations within the moiré structure. Moreover, STS studies have detected variations of p_z -orbitals which have been associated with spin texture in Pt-dichalcogenides.³⁵ This may indicate a lateral modulation of such spin textures within the moiré unit cell. Local magnetic properties may be studied by spin-resolved STS in the future.

METHODS

Experimental Details. PtTe_2 and PtSe_2 are grown in dedicated tellurium and selenium growth chambers by co-deposition of Pt and chalcogens. First a PtTe_2 multilayer film is grown at 300 °C substrate temperature on a freshly cleaved and vacuum-annealed HOPG

substrate.^{34,51} Subsequently, a monolayer of PtSe_2 is grown on top of the PtTe_2 at a growth temperature of 300 °C. For both compounds, Pt was evaporated in an e-beam evaporator from a 2 mm solid Pt rod. Tellurium was supplied from a Knudsen cell and selenium from a hot-wall valved cracker source. In either case, the chalcogen to Pt-flux ratio exceeded 10:1. The prepared films were characterized in a closed-cycle low-temperature STM with a base temperature close to 20 K. The bias voltage was applied to the sample, so the unoccupied and occupied states were recorded under positive and negative bias, respectively. dI/dV spectra were recorded with a lock-in amplifier with a 30 mV modulation voltage and the feedback loop turned off. The FER spectra were obtained from recording $Z-V$, with the feedback loop on, as a function of applied bias voltage, and dZ/dV was obtained by calculating the derivative numerically.

Computational. DFT calculations were performed using the Vienna Ab initio Simulation Package, within the plane-wave projector augmented-wave (PAW) method.^{52,53} The exchange-correlation functional was employed in the generalized gradient approximation of Perdew–Burke–Ernzerhof.⁵⁴ An energy cutoff of 400 eV was set for plane-wave expansion of the supercell calculations. van der Waals interactions were taken into account using the many-body dispersion combined with fractional ionic atoms method.⁵⁵ The effect of spin–orbit coupling is included in the electronic structure calculations. The Brillouin zone of the supercells was sampled using Gamma-point approximation. The charge densities were illustrated using the VESTA package.⁵⁶ The $\text{PtSe}_2/\text{PtTe}_2$ heterostructure was constructed by using an interface consisting of 13×13 unit cells of PtSe_2 and 12×12 unit cells of PtTe_2 monolayer corresponding to a lattice mismatch of only 0.9%. The supercell has a lattice constant of $a = b = 48.65 \text{ \AA}$ including 939 atoms.

ASSOCIATED CONTENT

SI Supporting Information

The Supporting Information is available free of charge at <https://pubs.acs.org/doi/10.1021/acsnano.2c12879>.

Figure S1: Evidence of cluster formation for multilayer growth of PtSe_2 on PtTe_2 . Figure S2: Relationship between atomic lattice rotation versus moiré unit cell rotation. Figure S3: Enlarged version of Fourier transformation of Figure 2c. Figure S4: STM images of mono- to trilayer thick PtSe_2 islands for determination of layer-dependent band gaps shown in Figure 2a. Figure S5: Comparison of dI/dV spectra taken in aligned and rotated moiré structures. Figure S6: STS spectra from Figure 2a,b replotted on a linear scale. Figure S7: Field emission resonance states measured in a rotated moiré structure. Figure S8: DFT calculations of density of

states in PtSe_2 supported on mono- and bilayer PtTe_2 . Figure S9: Estimation of band edge variations in the moiré unit cell from DFT calculations. Table S1: Calculated band gap (in eV) of various bilayers constructed from PtSe_2 and PtTe_2 monolayers (PDF)

AUTHOR INFORMATION

Corresponding Author

Matthias Batzill – Department of Physics, University of South Florida, Tampa, Florida 33620, United States;  orcid.org/0000-0001-8984-8427; Email: mbatzill@usf.edu

Authors

Jingfeng Li – Department of Physics, University of South Florida, Tampa, Florida 33620, United States

Mahdi Ghorbani-Asl – Institute of Ion Beam Physics and Materials Research, Helmholtz-Zentrum Dresden-Rossendorf, 01328 Dresden, Germany;  orcid.org/0000-0003-3060-4369

Kinga Lasek – Department of Physics, University of South Florida, Tampa, Florida 33620, United States

Vimukthi Pathirage – Department of Physics, University of South Florida, Tampa, Florida 33620, United States

Arkady V. Krasheninnikov – Institute of Ion Beam Physics and Materials Research, Helmholtz-Zentrum Dresden-Rossendorf, 01328 Dresden, Germany; Department of Applied Physics, Aalto University, 00076 Aalto, Finland;  orcid.org/0000-0003-0074-7588

Complete contact information is available at:

<https://pubs.acs.org/10.1021/acsnano.2c12879>

Notes

The authors declare no competing financial interest.

ACKNOWLEDGMENTS

Financial support from the National Science Foundation under award 2140038 is acknowledged. A.V.K. thanks the German Research Foundation (DFG) for support through Project KR 4866/6-1 and the collaborative research center “Chemistry of Synthetic 2D Materials” SFB-1415-417590517. The authors further thank the HZDR Computing Center, HLRS, Stuttgart, Germany, and TU Dresden Cluster “Taurus” for generous grants of CPU time.

REFERENCES

- (1) Dean, C. R.; Wang, L.; Maher, P.; Forsythe, C.; Ghahari, F.; Gao, Y.; Katoch, J.; Ishigami, M.; Moon, P.; Koshino, M.; Taniguchi, T.; Watanabe, K.; Shepard, K. L.; Hone, J.; Kim, P. Hofstadter’s Butterfly and the Fractal Quantum Hall Effect in Moiré Superlattices. *Nature* **2013**, *497*, 598–602.
- (2) Hunt, B.; Sanchez-Yamagishi, J. D.; Young, A. F.; Yankowitz, M.; LeRoy, B. J.; Watanabe, K.; Taniguchi, T.; Moon, P.; Koshino, M.; Jarillo-Herrero, P.; Ashoori, R. C. Massive Dirac Fermions and Hofstadter Butterfly in a van der Waals Heterostructure. *Science* **2013**, *340*, 1427–1430.
- (3) Cao, Y.; Fatemi, V.; Demir, A.; Fang, S.; Tomarken, S. L.; Luo, J. Y.; Sanchez-Yamagishi, J. D.; Watanabe, K.; Taniguchi, T.; Kaxiras, E.; Ashoori, R. C.; Jarillo-Herrero, P. Correlated Insulator Behaviour at Half-Filling in Magic-Angle Graphene Superlattices. *Nature* **2018**, *556*, 80–84.
- (4) Cao, Y.; Fatemi, V.; Fang, S.; Watanabe, K.; Taniguchi, T.; Kaxiras, E.; Jarillo-Herrero, P. Unconventional Superconductivity in Magic-Angle Graphene Superlattices. *Nature* **2018**, *556*, 43–50.

(5) Cao, Y.; Rodan-Legrain, D.; Rubies-Bigorda, O.; Park, J. M.; Watanabe, K.; Taniguchi, T.; Jarillo-Herrero, P. Tunable Correlated States and Spin-Polarized Phases in Twisted Bilayer–Bilayer Graphene. *Nature* **2020**, *583*, 215–220.

(6) Zhang, C.; Chuu, C.-P.; Ren, X.; Li, M.-Y.; Li, L.-J.; Jin, C.; Chou, M.-Y.; Shih, C.-K. Interlayer Couplings, Moiré Patterns, and 2D Electronic Superlattices in $\text{MoS}_2/\text{WSe}_2$ Hetero-Bilayers. *Sci. Adv.* **2017**, *3*, e1601459.

(7) Susarla, S.; Sassi, L. M.; Zobelli, A.; Woo, S. Y.; Tizei, L. H. G.; Stéphan, O.; Ajayan, P. M. Mapping Modified Electronic Levels in the Moiré Patterns in $\text{MoS}_2/\text{WSe}_2$ Using Low-Loss EELS. *Nano Lett.* **2021**, *21*, 4071–4077.

(8) Li, H.; Li, S.; Naik, M. H.; Xie, J.; Li, X.; Wang, J.; Regan, E.; Wang, D.; Zhao, W.; Zhao, S.; Kahn, S.; Yumigeta, K.; Blei, M.; Taniguchi, T.; Watanabe, K.; Tongay, S.; Zettl, A.; Louie, S. G.; Wang, F.; Crommie, M. F. Imaging Moiré Flat Bands in Three-Dimensional Reconstructed WSe_2/WS_2 Superlattices. *Nat. Mater.* **2021**, *20*, 945–950.

(9) Waters, D.; Nie, Y.; Lüpke, F.; Pan, Y.; Fölsch, S.; Lin, Y.-C.; Jariwala, B.; Zhang, K.; Wang, C.; Lv, H.; Cho, K.; Xiao, D.; Robinson, J. A.; Feenstra, R. M. Flat Bands and Mechanical Deformation Effects in the Moiré Superlattice of $\text{MoS}_2/\text{WSe}_2$ Heterobilayers. *ACS Nano* **2020**, *14*, 7564–7573.

(10) Pan, Y.; Fölsch, S.; Nie, Y.; Waters, D.; Lin, Y.-C.; Jariwala, B.; Zhang, K.; Cho, K.; Robinson, J. A.; Feenstra, R. M. Quantum-Confining Electronic States Arising from the Moiré Pattern of $\text{MoS}_2/\text{WSe}_2$ Heterobilayers. *Nano Lett.* **2018**, *18*, 1849–1855.

(11) Regan, E. C.; Wang, D.; Paik, E. Y.; Zeng, Y.; Zhang, L.; Zhu, J.; MacDonald, A. H.; Deng, H.; Wang, F. Emerging Exciton Physics in Transition Metal Dichalcogenide Heterobilayers. *Nat. Rev. Mater.* **2022**, *7*, 778–795.

(12) Gogoi, P. K.; Lin, Y.-C.; Senga, R.; Komsa, H.-P.; Wong, S. L.; Chi, D.; Krasheninnikov, A. V.; Li, L.-J.; Breese, M. B. H.; Pennycook, S. J.; Wee, A. T. S.; Suenaga, K. Layer Rotation-Angle-Dependent Excitonic Absorption in van der Waals Heterostructures Revealed by Electron Energy Loss Spectroscopy. *ACS Nano* **2019**, *13*, 9541–9550.

(13) Pivetta, M.; Patthey, F.; Stengel, M.; Baldereschi, A.; Schneider, W.-D. Local work function Moiré pattern on ultrathin ionic films: NaCl on $\text{Ag}(100)$. *Phys. Rev. B* **2005**, *72*, 115404.

(14) Rienks, E. D. L.; Nilius, N.; Rust, H.-P.; Freund, H.-J. Surface Potential of a Polar Oxide Film: FeO on $\text{Pt}(111)$. *Phys. Rev. B* **2005**, *71*, 241404.

(15) Dahal, A.; Batzill, M. Growth from Behind: Intercalation-Growth of Two-Dimensional FeO Moiré Structure Underneath of Metal-Supported Graphene. *Sci. Rep.* **2015**, *5*, 11378.

(16) Kim, H.; Hasegawa, Y. Spatial variation in local work function as an origin of moiré contrast in scanning tunneling microscopy images of Pb thin films/Si(111). *Jpn. J. Appl. Phys.* **2016**, *55*, 08NA03.

(17) Wang, B.; Caffio, M.; Bromley, C.; Frücht, H.; Schaub, R. Coupling Epitaxy, Chemical Bonding, and Work Function at the Local Scale in Transition Metal-Supported Graphene. *ACS Nano* **2010**, *4*, 5773–5782.

(18) Corso, M.; Auwärter, W.; Muntwiler, M.; Tamai, A.; Greber, T.; Osterwalder, J. Boron Nitride Nanomesh. *Science* **2004**, *303*, 217–220.

(19) Goriachko, A.; He, K.; Knapp, M.; Over, H.; Corso, M.; Brugger, T.; Berner, S.; Osterwalder, J.; Greber, T. Self-Assembly of a Hexagonal Boron Nitride Nanomesh on Ru(0001). *Langmuir* **2007**, *23*, 2928–2931.

(20) Joshi, S.; Ecija, D.; Koitz, R.; Iannuzzi, M.; Seitsonen, A. P.; Hutter, J.; Sachdev, H.; Vijayaraghavan, S.; Bischoff, F.; Seufert, K.; Barth, J. V.; Auwärter, W. Boron Nitride on $\text{Cu}(111)$: An Electronically Corrugated Monolayer. *Nano Lett.* **2012**, *12*, 5821–5828.

(21) Zhang, Q.; Yu, J.; Ebert, P.; Zhang, C.; Pan, C.-R.; Chou, M.-Y.; Shih, C.-K.; Zeng, C.; Yuan, S. Tuning Band Gap and Work Function Modulations in Monolayer hBN/Cu(111) Heterostructures with Moiré Patterns. *ACS Nano* **2018**, *12*, 9355–9362.

(22) zum Hagen, F. H. F.; Zimmermann, D. M.; Silva, C. C.; Schlueter, C.; Atodiresei, N.; Jolie, W.; Martínez-Galera, A. J.; Dombrowski, D.; Schröder, U. A.; Will, M.; Lazić, P.; Caciuc, V.; Blügel, S.; Lee, T.-L.; Michely, T.; Busse, C. Structure and Growth of Hexagonal Boron Nitride on Ir(111). *ACS Nano* **2016**, *10*, 11012–11026.

(23) Auwärter, W. Hexagonal Boron Nitride Monolayers on Metal Supports: Versatile Templates for Atoms, Molecules and Nanostructures. *Surf. Sci. Rep.* **2019**, *74*, 1–95.

(24) Zhang, Q.; Chen, Y.; Zhang, C.; Pan, C.-R.; Chou, M.-Y.; Zeng, C.; Shih, C.-K. Bandgap renormalization and work function tuning in MoSe₂/hBN/Ru(0001) heterostructures. *Nat. Commun.* **2016**, *7*, 13843.

(25) Zhang, L.; Yang, T.; Sahdan, M. F.; Arramel; Xu, W.; Xing, K.; Feng, Y. P.; Zhang, W.; Wang, Z.; Wee, A. T. S. Precise Layer-Dependent Electronic Structure of MBE-Grown PtSe₂. *Adv. Electr. Mater.* **2021**, *7*, 2100559.

(26) Zhang, L.; Yang, T.; Arramel; Feng, Y. P.; Wee, A. T. S.; Wang, Z. MBE-Grown Ultrathin PtTe₂ Film and the Layer-Dependent Electronic Structure. *Nanoscale* **2022**, *14*, 7650–7658.

(27) Lasek, K.; Li, J.; Kolekar, S.; Coelho, P. M.; Zhang, M.; Wang, Z.; Batzill, M. Synthesis and Characterization of 2D Transition Metal Dichalcogenides: Recent Progress from a Vacuum Surface Science Perspective. *Surf. Sci. Rep.* **2021**, *76*, 100523.

(28) Villaos, R. A. B.; Crisostomo, C. P.; Huang, Z.-Q.; Huang, S.-M.; Padama, A. A. B.; Alba, M. A.; Lin, H.; Chuang, F.-C. Thickness Dependent Electronic Properties of Pt Dichalcogenides. *npj 2D Mater. Appl.* **2019**, *3*, 2.

(29) Lin, M.-K.; Villaos, R. A. B.; Hlevyack, J. A.; Chen, P.; Liu, R.-Y.; Hsu, C.-H.; Avila, J.; Mo, S.-K.; Chuang, F.-C.; Chiang, T. C. Dimensionality-Mediated Semimetal-Semiconductor Transition in Ultrathin PtTe₂ Films. *Phys. Rev. Lett.* **2020**, *124*, 036402.

(30) Li, J.; Kolekar, S.; Ghorbani-Asl, M.; Lehnert, T.; Biskupek, J.; Kaiser, U.; Krasheninnikov, A. V.; Batzill, M. Layer-Dependent Band Gaps of Platinum Dichalcogenides. *ACS Nano* **2021**, *15*, 13249–13259.

(31) Lasek, K.; Ghorbani-Asl, M.; Pathirage, V.; Krasheninnikov, A. V.; Batzill, M. Controlling Stoichiometry in Ultrathin van der Waals Films: PtTe₂, Pt₂Te₃, Pt₃Te₄, and Pt₂Te₂. *ACS Nano* **2022**, *16*, 9908–9919.

(32) Yao, W.; Wang, E.; Huang, H.; Deng, K.; Yan, M.; Zhang, K.; Miyamoto, K.; Okuda, T.; Li, L.; Wang, Y.; Gao, H.; Liu, C.; Duan, W.; Zhou, S. Direct Observation of Spin-Layer Locking by Local Rashba Effect in Monolayer Semiconducting PtSe₂ Film. *Nat. Commun.* **2017**, *8*, 14216.

(33) Lichtenstein, L.; Heyde, M.; Ulrich, S.; Nilius, N.; Freund, H.-J. Probing the Properties of Metal–Oxide Interfaces: Silica Films on Mo and Ru Supports. *J. Phys.: Condens. Matter* **2012**, *24*, 354010.

(34) Ploigt, H. C.; Brun, C.; Pivetta, M.; Patthey, F.; Schneider, W.-D. Local Work Function Changes Determined by Field Emission Resonances: NaCl/Ag(100). *Phys. Rev. B* **2007**, *76*, 195404.

(35) Ruggiero, C. D.; Choi, T.; Gupta, J. A. Tunneling Spectroscopy of Ultrathin Insulating Films: CuN on Cu(100). *Appl. Phys. Lett.* **2007**, *91*, 253106.

(36) Ruffieux, P.; Aït-Mansour, K.; Bendounan, A.; Fasel, R.; Patthey, L.; Gröning, P.; Gröning, O. Mapping the Electronic Surface Potential of Nanostructured Surfaces. *Phys. Rev. Lett.* **2009**, *102*, 086807.

(37) Zhao, P.; Wan, Y.; Zhang, S.; Gao, A.; Guo, P.; Jiang, Z.; Zheng, J. Strain Effects on the 2D van der Waals Heterostructure C3B/C3N: A Density Functional Theory and a Tight-Binding Study. *Phys. Status Solidi RRL* **2020**, *14*, 2000012.

(38) Joshi, S.; Bischoff, F.; Koitz, R.; Ecija, D.; Seufert, K.; Seitsonen, A. P.; Hutter, J.; Diller, K.; Urgel, J. I.; Sachdev, H.; Barth, J. V.; Auwärter, W. Control of Molecular Organization and Energy Level Alignment by an Electronically Nanopatterned Boron Nitride Template. *ACS Nano* **2014**, *8*, 430–442.

(39) Schulz, F.; Drost, R.; Hämäläinen, S. K.; Liljeroth, P. Templated Self-Assembly and Local Doping of Molecules on Epitaxial Hexagonal Boron Nitride. *ACS Nano* **2013**, *7*, 11121–11128.

(40) Joshi, S.; Bischoff, F.; Koitz, R.; Ecija, D.; Seufert, K.; Seitsonen, A. P.; Hutter, J.; Diller, K.; Urgel, J. I.; Sachdev, H.; Barth, J. V.; Auwärter, W. Control of Molecular Organization and Energy Level Alignment by an Electronically Nanopatterned Boron Nitride Template. *ACS Nano* **2014**, *8*, 430–442.

(41) Urgel, J. I.; Schwarz, M.; Garnica, M.; Stassen, D.; Bonifazi, D.; Ecija, D.; Barth, J. V.; Auwärter, W. Controlling Coordination Reactions and Assembly on a Cu(111) Supported Boron Nitride Monolayer. *J. Am. Chem. Soc.* **2015**, *137*, 2420–2423.

(42) Widmer, R.; Passerone, D.; Mattle, T.; Sachdev, H.; Gröning, O. Probing the Selectivity of a Nanostructured Surface by Xenon Adsorption. *Nanoscale* **2010**, *2*, 502–508.

(43) Pörtner, M.; Wei, Y.; Riss, A.; Seufert, K.; Garnica, M.; Barth, J. V.; Seitsonen, A. P.; Diekhöner, L.; Auwärter, W. Charge State Control of F₁₆CoPc on h-BN/Cu(111). *Adv. Mater. Interface* **2020**, *7*, 2000080.

(44) Liu, L.; Dienel, T.; Widmer, R.; Gröning, O. Interplay Between Energy-Level Position and Charging Effect of Manganese Phthalocyanines on an Atomically Thin Insulator. *ACS Nano* **2015**, *9*, 10125–10132.

(45) Chia, X.; Adriano, A.; Lazar, P.; Sofer, Z.; Luxa, J.; Pumera, M. Layered Platinum Dichalcogenides (PtS₂, PtSe₂, and PtTe₂) Electrocatalysis: Monotonic Dependence on the Chalcogen Size. *Adv. Funct. Mater.* **2016**, *26*, 4306–4318.

(46) Rosli, N. F.; Mayorga-Martinez, C. C.; Latiff, N. M.; Rohaizad, N.; Sofer, Z.; Fisher, A. C.; Pumera, M. Layered PtTe₂ Matches Electrocatalytic Performance of Pt/C for Oxygen Reduction Reaction with Significantly Lower Toxicity. *ACS Sustain. Chem. Eng.* **2018**, *6*, 7432–7441.

(47) Huang, H.; Fan, X.; Singh, D. J.; Zheng, W. Modulation of Hydrogen Evolution Catalytic Activity of Basal Plane in Monolayer Platinum and Palladium Dichalcogenides. *ACS Omega* **2018**, *3*, 10058–10065.

(48) Clark, O. J.; Mazzola, F.; Feng, J.; Sunko, V.; Markovic, I.; Bawden, L.; Kim, T. K.; King, P. D. C.; Bahramy, M. S. Dual Quantum Confinement and Anisotropic Spin Splitting in the Multivalley Semimetal PtSe₂. *Phys. Rev. B* **2019**, *99*, 045438.

(49) Avsar, A.; Ciarrocchi, A.; Pizzochero, M.; Unuchek, D.; Yazyev, O. V.; Kis, A. Defect Induced, Layer-Modulated Magnetism in Ultrathin Metallic PtSe₂. *Nat. Nanotechnol.* **2019**, *14*, 674–678.

(50) Avsar, A.; Cheon, C.-Y.; Pizzochero, M.; Tripathi, M.; Ciarrocchi, A.; Yazyev, O. Y.; Kis, A. Probing Magnetism in Atomically Thin Semiconducting PtSe₂. *Nat. Commun.* **2020**, *11*, 4806.

(51) Lasek, K.; Li, J.; Ghorbani-Asl, M.; Khatun, S.; Alanwoko, O.; Pathirage, V.; Krasheninnikov, A. V.; Batzill, M. Formation of In-Plane Semiconductor–Metal Contacts in 2D Platinum Telluride by Converting PtTe₂ to Pt₂Te₂. *Nano Lett.* **2022**, *22*, 9571–9577.

(52) Kresse, G.; Furthmüller, J. Efficiency of Ab-Initio Total Energy Calculations for Metals and Semiconductors Using a Plane-Wave Basis Set. *Comput. Mater. Sci.* **1996**, *6*, 15–50.

(53) Kresse, G.; Furthmüller, J. Efficient Iterative Schemes for Ab Initio Total-Energy Calculations Using a Plane-Wave Basis Set. *Phys. Rev. B* **1996**, *54*, 11169–11186.

(54) Perdew, J. P.; Burke, K.; Ernzerhof, M. Generalized Gradient Approximation Made Simple. *Phys. Rev. Lett.* **1996**, *77*, 3865–3868.

(55) Tawfik, S. A.; Gould, T.; Stampfl, C.; Ford, M. J. Evaluation of van der Waals Density Functionals for Layered Materials. *Phys. Rev. Mater.* **2018**, *2*, 034005.

(56) Momma, K.; Izumi, F. VESTA: A Three-Dimensional Visualization System for Electronic and Structural Analysis. *J. Appl. Crystallogr.* **2008**, *41*, 653–658.